ELSEVIER

Earth and Planetary Science Letters 203 (2002) 557–566

EPSL

www.elsevier.com/locate/epsl

Elasticity of $(Mg_{0.83},Fe_{0.17})O$ ferropericlase at high pressure: ultrasonic measurements in conjunction with X-radiation techniques

Jennifer Kung [a,*], Baosheng Li [a], Donald J. Weidner [a,b], Jianzhong Zhang [a], Robert C. Liebermann [a,b]

[a] *Mineral Physics Institute, Stony Brook University, Stony Brook, NY 11794-2100, USA*
[b] *Department of Geosciences, Stony Brook University, Stony Brook, NY 11794-2100, USA*

Received 13 March 2002; received in revised form 1 May 2002; accepted 10 July 2002

Abstract

The elasticity of ferropericlase with a potential mantle composition of $(Mg_{0.83},Fe_{0.17})O$ is determined using ultrasonic interferometry in conjunction with in situ X-radiation techniques (X-ray diffraction and X-radiography) in a DIA-type cubic anvil high-pressure apparatus to pressures of 9 GPa (NaCl pressure scale) at room temperature. In this study, we demonstrate that it is possible to directly monitor the specimen length using an X-ray image technique and show that these lengths are consistent with those derived from X-ray diffraction data when no plastic deformation of the specimen occurs during the experiment. By combining the ultrasonic and X-ray diffraction data, the adiabatic elastic bulk (K_S) and shear (G) moduli and specimen volume can be measured simultaneously. This enables pressure scale-free measurements of the equation of state of the specimen using a parameterization such as the Birch–Murnaghan equation of state. The elastic moduli determined for $(Mg_{0.83},Fe_{0.17})O$ are $K_{S0} = 165.5(12)$ GPa, $G_0 = 112.4(4)$ GPa, and their pressure derivatives are $K_{S0}' = 4.17(20)$ and $G_0' = 1.89(6)$. If these results are compared with those for MgO, they demonstrate that K_{S0} and K_{S0}' are insensitive to the addition of 17 mol% FeO, but G_0 and G_0' are reduced by 14% and 24%, respectively. We calculate that the P and S wave velocities of a perovskite plus ferropericlase phase assemblage with a pyrolite composition at the top of the lower mantle (660 km depth) are lowered by 0.8 and 2.3%, respectively, when compared with those calculated using the elastic properties of end-member MgO. Consequently, the magnitudes of the calculated wave velocity jumps across the 660 km discontinuity are reduced by about 11% for P wave and 20% for S wave, if this discontinuity is considered as a phase transformation boundary only (ringwoodite → perovskite+ferropericlase).

Keywords: periclase; elastic properties; high pressure; X-ray analysis; lower mantle; iron-rich composition

1. Introduction

Ferropericlase, (Mg,Fe)O, is widely believed to be a major phase in the lower mantle of the Earth, coexisting with orthorhombic silicate perovskite, $(Mg,Fe,Al)SiO_3$. Experiments on Mg/Fe

* Corresponding author. Tel.: +1-631-632-8338; Fax: +1-631-632-8140.
E-mail address: jkung@notes.cc.sunysb.edu (J. Kung).

0012-821X/02/$ – see front matter © 2002 Elsevier Science B.V. All rights reserved.
PII: S0012-821X(02)00838-5

partitioning at high pressures suggest that the FeO content in this ferropericlase phase lies in the range 10–20 mol% for potential compositional models of the Earth's interior (e.g. [1–3]). To date, elasticity studies on the effect of the Fe substitution into MgO-periclase [4–6] were conducted at ambient or low-pressure conditions. Static compression studies have explored higher pressure behavior, but provided only indirect determination of the isothermal bulk modulus (K_{T0}) and its pressure derivatives (K_{T0}'), and no information on the shear properties [6–9]. Bonczar and Graham [5] have reported the pressure and temperature derivatives of elastic moduli for entire (Mg,Fe)O solid solution series using ultrasonic techniques but under experimental conditions up to only 0.5 GPa and 75°C. Ultrasonic interferometric techniques employed in a multi-anvil, high-pressure apparatus in our laboratory have extended the accessible experimental range of such ultrasonic experiments to $P = 10$ GPa and $T = 1200$°C [10].

The key parameters needed to determine the elastic wave velocities (V_P and V_S) and the bulk (K_S) and shear (G) moduli using ultrasonic techniques are the travel times, sample length and specimen density. Using the phase comparison method of ultrasonic interferometry, travel times can be measured with a precision ranging from 10^{-3} to 10^{-6} [11,12]. In the absence of in situ measurements of specimen length by X-radiation or other methods, many previous studies have relied on approaches such as that of Cook [13,14] (which employs the measured travel times to infer compressibility which in turn is used to calculate pressure-induced changes in length), or on separate experiments to determine the thermal expansion at high temperature [15]. By using in situ X-ray diffraction in conjunction with the ultrasonic measurements [16,17], it has been possible to infer the specimen length (on the assumptions that the bulk sample strain is isotropic and purely elastic) from the measurement of the unit cell volume at elevated pressures and temperatures and thereby study the elasticity of important mantle minerals [18–20]. More recently, X-ray radiographic imaging techniques have been developed to observe specimen lengths directly at high pressures and temperatures, therefore enabling the travel time data to be converted to velocities and moduli directly [21].

We report here the results of one of the first experimental studies using these combined capabilities, providing new data on the elasticity of $(Mg_{0.83},Fe_{0.17})O$ ferropericlase at pressures up to 9 GPa (as determined from the NaCl pressure scale) at room temperature. We also explore the influence of the new data on the seismic profiles at the lower mantle conditions in terms of pyrolite as a potential model for the chemical composition of the Earth's mantle.

2. Materials and methods

2.1. Starting materials

A composition of ferropericlase with 17 mol% FeO was chosen for the study because it is within the predicted range of compositions for this mineralogical constituent in the lower mantle. Another advantage of this composition is its high absorption of X-rays, when compared with the adjacent materials (Al_2O_3 and NaCl); this contrast generates a sharp image for our experimental radiography studies (see details below and in Fig. 1). There is no evidence that a phase transition occurs for the composition of $(Mg_{0.83},Fe_{0.17})O$ under the P–T conditions of our experiments (up to 10 GPa, ~1000°C).

A mixture of $MgO+Fe_2O_3$ (0.83:0.085 molar ratio) was pressed into pellets and then heated at 1200°C and log $fO_2 = -10.8$ bar for 24 h. The process was repeated until the final product was confirmed as ferropericlase by X-ray diffraction, with a cell parameter of $a = 4.235(1)$ Å. The value is consistent with that for the composition of $(Mg_{0.83},Fe_{0.17})O$ of $a = 4.233$ Å, which is based on the relationship of the cell parameter and $\Sigma Fe/(\Sigma Fe+Mg)$ for (Mg,Fe)O solid solution in the compositional range $\Sigma Fe/(\Sigma Fe+Mg) = 0$–$0.24$, and containing $Fe^{3+}/\Sigma Fe < 0.02$ [6].

2.2. Hot-pressing of polycrystalline specimens

The methods for hot-pressing polycrystalline aggregates at high pressure in a uniaxial split-cyl-

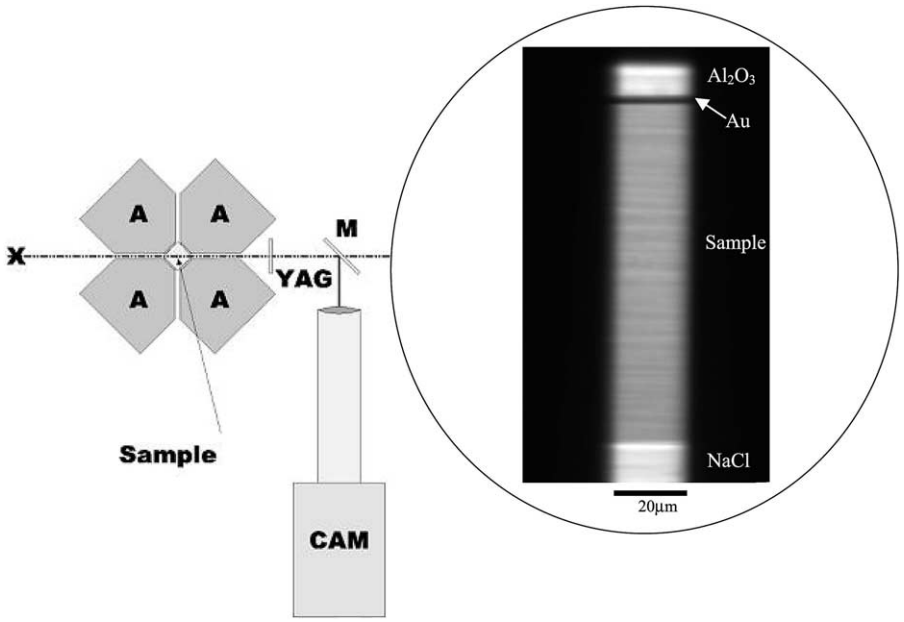

Fig. 1. X-radiographic image system (after Vaughan et al. [29]). The X-rays (X) pass through the gaps between the anvils (A) in the high-pressure apparatus (SAM85, DIA-type apparatus) and into the sample chamber. The transmitted X-rays illuminate a YAG crystal (YAG), where an image of the cell assembly is generated. Then the image is reflected by a mirror (M) into the CCD camera (CAM). A typical cell assembly image observed in our experiment is shown on the right panel; (from top to bottom) the Al_2O_3 acoustic buffer rod, a 2 microns thick gold foil inserted between buffer rod and specimen, a NaCl disk behind the specimen.

inder apparatus (USCA-1000 [22]) have been described in previous studies from our laboratory [23,24]. We utilized a 14/8 mm cell assembly modified from Gwanmesia et al. [25] for hot-pressing the polycrystalline specimen of ferropericlase in this study. The starting material (Mg,Fe)O was loaded into an iron capsule and hot-pressed at a pressure of ~10 GPa and 1000°C for 1~2 h. The experiment was terminated by decreasing the pressure and temperature simultaneously and slowly over a period of 12 h in order to relax intragranular stresses in the polycrystalline aggregates. Analysis using an electron microprobe with back-scattering imaging indicates an average grain size of 20 microns and chemical composition unchanged from the starting materials (under the assumption that all Fe was Fe^{2+}). The cell parameter of the hot-pressed polycrystalline specimen was identical to that of the starting material within the experimental uncertainty (0.001 Å). Combining these data, one obtains a theoretical density of 3.994(2) g cm^{-3}. Using the Archimedes' immersion technique, the bulk density of specimen is 3.99(4) g cm^{-3} (or 99.9% of the X-ray value).

The cell parameter of (Mg,Fe)O was also determined after ultrasonic measurement (up to 11 GPa, with eight heating cycles up to 600°C, see Section 2.3) to be $a = 4.233(1)$ Å. As this was unchanged from that of the starting material ($a = 4.235(1)$ Å), we conclude that no change in either the $\Sigma Fe/(\Sigma Fe+Mg)$ or $Fe^{3+}/\Sigma Fe$ ratios occurred during the course of our hot-pressing and ultrasonic experiments.

2.3. Ultrasonic measurements

Two-way travel times of ultrasonic wave through the polycrystalline specimens were collected using an ANUTEC interferometer with a buffer-rod assembly and phase comparison method [14,26]. $LiNbO_3$ transducers (overtone-polished parallel-plated) were used both as source and receiver of the ultrasonic signals. In this

study, dual-mode transducers, 10° rotated *Y*-cut (which generates P and S stress waves at the same time; 50 MHz resonant frequency for P wave and 30 MHz for S wave), were used in the high-pressure experiment. Use of this type of transducer saves experimental time and prevents the introduction of systematic uncertainties in the interpretation of data from separate P and S wave measurements using single-mode transducers [27].

Ultrasonic measurements at high pressure were performed using a DIA-type, large-volume apparatus (SAM85) in conjunction with in situ X-ray radiation techniques [28], installed at superconducting wiggler beamline X17B of National Synchrotron Light Source at the Brookhaven National Laboratory. An energy-dispersive X-ray method using white radiation was employed to collect the diffraction patterns for both the specimen and NaCl (which was used as a reference pressure marker). In this study, we used a $6\times6\times6$ mm^3 cell assembly with a mixture of amorphous boron and epoxy resin as the pressure medium and a graphite furnace to generate the high temperature environment [16–20]. A W/Re 3%–W/Re 25% thermocouple located at the center of furnace and in direct contact with unjacketed specimen provided the measurement of temperature, and a disk of NaCl provided the hydrostatic environment and also served as a pressure calibrant (for details see figure 20 in reference [17]). Although the original plan was to conduct the ultrasonic measurements at simultaneous high pressure and high temperature, the thermocouple failed at peak pressure ($\sim$11 GPa), $\sim$600°C during the first heating cycle, thereby preventing precise temperature measurements in the subsequent heating/cooling cycles. Consequently, for the remainder of the experiment, the temperatures were estimated by the power–temperature relationship obtained from the first heating cycle. By heating the cell assembly to $\sim$500–600°C at each pressure during decompression, the macroscopic deviatoric stress imposed on the specimen by pressure medium was minimized. The acoustic travel times as a function of pressure were then collected at room temperature along the decompression path (see figure 1 in reference [20] for typical *P*–*T* path).

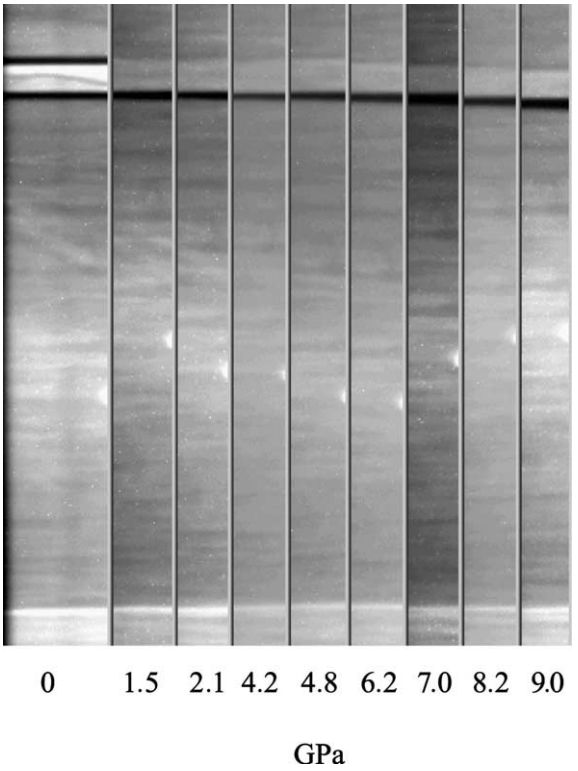

Fig. 2. A series of X-ray images recorded at pressures from ambient to 9.0 GPa (indicated by the NaCl pressure scale). The images shown here are the same as in Fig. 1 (from top to the bottom: Al_2O_3 buffer rod, gold foil, specimen and NaCl).

The acoustic pathway for travel time measurements at high pressure is a sandwiched assembly, consisting of a WC cube, a polycrystalline Al_2O_3 (Coors 998) buffer rod, specimen and a disk of NaCl (Fig. 1); a thin gold foil (2 microns thick) was used to improve the acoustic coupling between interfaces. Bond corrections have been made for all travel times measured in this work by following the procedure described by Niesler and Jackson [26]. The average round-trip travel time for P wave was averaged from 45 to 65 MHz and S wave from 25 to 35 MHz.

2.4. *X-radiographic image technique*

In the SAM85 apparatus, the X-ray beam passes though the gaps between anvils and then the cell assembly, and illuminates a fluorescent

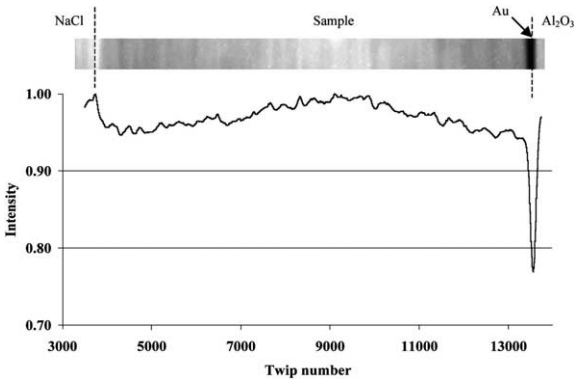

Fig. 3. Image file read as gray-scale (normalized intensity) on the Y axis, and the twip numbers on the X axis. Two clear interfaces are shown in the image: darkest (on the right, lower intensity area) and brightest (on the left, higher intensity area) are the gold foil and the boundary of specimen and NaCl, respectively.

YAG crystal (Fig. 1). The visible light generated by the YAG crystal is reflected by a mirror into the CCD camera where an image of the cell assembly is captured [29]. A typical X-ray image of the cell assembly in our experiment is shown on the right panel of Fig. 1, consisting (from top to bottom) of the Al_2O_3 acoustic buffer rod, gold foil, the specimen and the NaCl disk. The contrasting intensities at different regions are caused by the difference in the X-ray absorption of these materials. A sequence of X-ray images have been recorded during the course of collecting ultrasonic data at high pressures (Fig. 2). The final image taken at ambient conditions when the press was open, and along with the measured length of the recovered specimen after high-pressure run, provides the conversion factor between the actual specimen dimension and images.

An output file of intensities along the specimen region was obtained for each image (Fig. 3). The specimen region is defined by the discontinuity in intensity at both boundaries. The interface between sample and backing material (NaCl) has the highest intensity, and at the other end, the gold foil has the lowest intensity. In order to resolve sub-pixel changes between sequential images, a measuring unit 'twip' was used to read out the intensity instead of pixel (on the display resolution these images were analyzed, one pixel was represented by 12 twips). The relative specimen length change from one condition to another was measured by the change of twips needed to obtain the best correlation of the two boundaries of the specimen. Using the converting factor, the absolute specimen lengths at all experimental conditions were subsequently calculated. The precision of this direct measurement of specimen length is estimated to be 0.1%.

3. Experimental data

The diffraction peaks (111), (200), (220), (311) and (222) of (Mg,Fe)O collected during the experiment were used to determine the cell volume (V) at ambient conditions and high pressures, therefore, the specimen densities were also determined ($\rho = \rho_0(V_0/V)$, where V_0 is the unit cell volume at ambient conditions). The cubic root of the ratio of the cell volume change ($S = (V_0/V)^{1/3}$, linear compression) was used to calculate the length of the specimen under the experimental conditions ($l_{(P-V\ \mathrm{data})} = l_0/S$). Using the X-radiographic imaging technique described above, we also measured

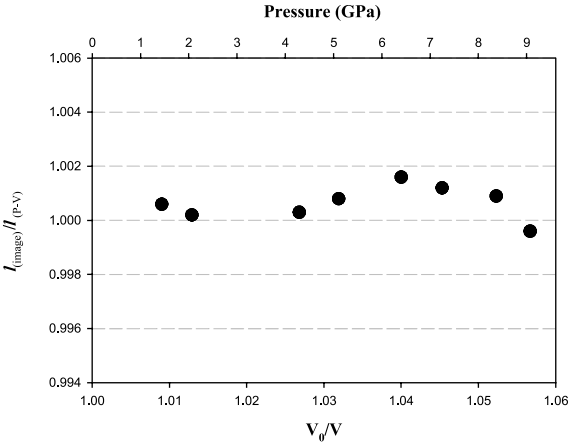

Fig. 4. Ratio of observed and calculated specimen lengths plotted as a function of pressure (NaCl as pressure calibrant) (top X axis) and of V_0/V of the specimen (bottom X axis). The observed specimen lengths ($l_{(\mathrm{image})}$) were obtained from the X-radiographic imaging technique; the calculated ones ($l_{(P-V)}$) are derived from the X-ray diffraction data (P–V data). When this ratio is equal to one, we can conclude that all of the specimen deformation is elastic and occurs isotropically under compression and expansion.

the axial length of cylindrical specimens under the same experimental conditions. These two length measurements are tabulated in Table 1 and agree within 2 microns for all experimental conditions. In Fig. 4, we plot the ratio ($l_{(\mathrm{image})}/l_{(P-V\ \mathrm{data})}$) of these two measurements of the relative length changes. If all of the observed length changes are the result of isotropic compression or expansion as the specimen deforms elastically, then this ratio should be equal to 1. We see in Fig. 4 that this assumption is indeed verified for our experimental data and, thus, we could confidently utilize either length measurement to convert the measured travel times to velocities.

Travel times of P and S waves of the (Mg,Fe)O specimen at high pressure were tabulated in Table 1 and plotted in Fig. 5 as a function of V_0/V of (Mg,Fe)O. These travel times, as well as X-ray density, specimen lengths and V_0/V data (Table 2), have been used to calculate the longitudinal (L, calculated from t_P) and shear (G, calculated from t_S) moduli at pressures using the following equations:

$$L, G = 4\rho_0 l_0^2 \left(\frac{1}{t^2_{(S,P)}}\right)\left(\frac{V_0}{V}\right)^{1/3} \quad (1)$$

and

$$L, G = 4\rho_0 l^2 \left(\frac{1}{t^2_{(S,P)}}\right)\left(\frac{V_0}{V}\right) \quad (2)$$

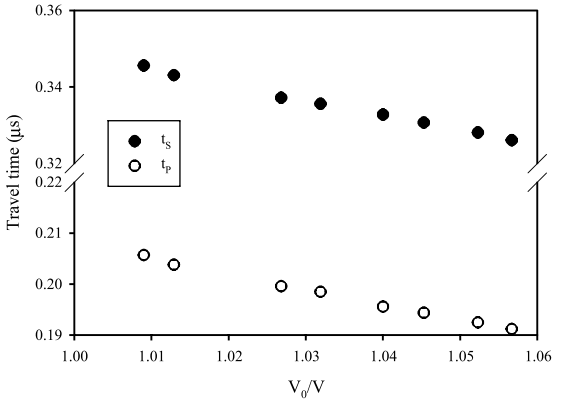

Fig. 5. P and S wave travel times of $(Mg_{0.83},Fe_{0.17})O$ plotted as a function of V_0/V of the specimen.

Elastic moduli were calculated using Eq. 1 when the specimen length was derived using P–V data only and Eq. 2 when the axial length was observed directly from the X-ray image. The elastic moduli calculated using the sample length obtained from both methods (using Eqs. 1 and 2) are in good agreement within their mutual uncertainties ($<0.5\%$) (Fig. 6).

We have fitted both sets of moduli data in Fig. 6 to third-order Eulerian finite-strain equations:

$$L = \rho V_P^2 = S^5\left[L_1 + \frac{1}{2}L_2(1-S^2)\right] \quad (3)$$

$$G = \rho V_S^2 = S^5\left[M_1 + \frac{1}{2}M_2(1-S^2)\right] \quad (4)$$

Table 1
Sample $(Mg_{0.83},Fe_{0.17})O$, K533, volumes and lengths and elastic wave travel times at high pressures

Pressure[a] (GPa)	V_0/V	Travel time (μs)		Length (mm)	
		P	S	Image	X-ray data
1.54	1.0090(2)	0.2057(4)	0.3456(4)	0.923	0.922
2.06	1.0129(3)	0.2038(3)	0.3431(7)	0.921	0.921
4.29	1.0268(5)	0.1996(6)	0.3372(5)	0.917	0.917
4.84	1.0319(3)	0.1985(1)	0.3356(2)	0.916	0.915
6.20	1.0400(4)	0.1956(2)	0.3328(3)	0.915	0.913
7.01	1.0453(3)	0.1944(2)	0.3307(6)	0.913	0.911
8.24	1.0523(7)	0.1925(5)	0.3218(4)	0.910	0.909
9.04	1.0567(9)	0.1912(4)	0.3261(6)	0.908	0.908

[a] The pressure scale readings are derived using NaCl pressure standard.
Sample cell volume (V_0) used here was 75.8374 (222) Å^3, collected when press opened after the experiment finished. Sample length (l_0) was 0.925(1) mm after the experiment.

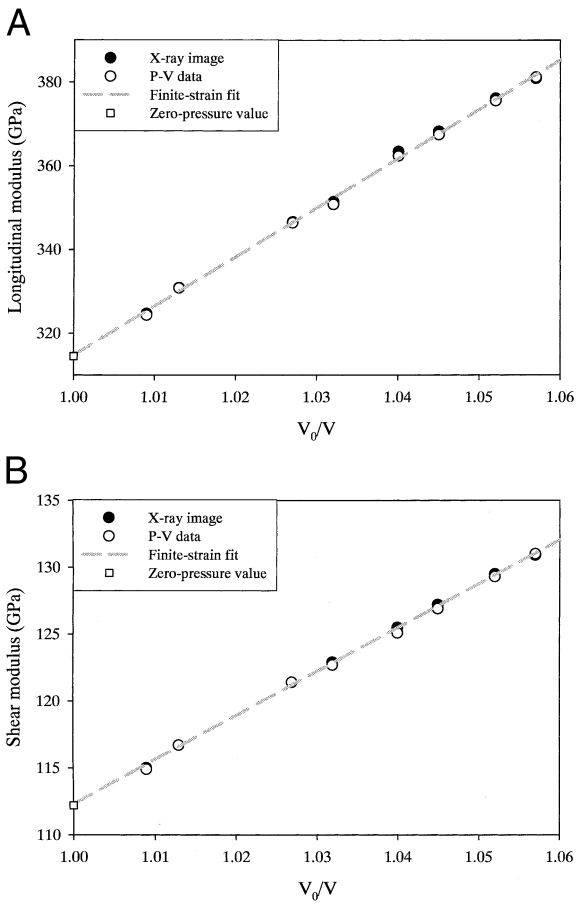

Fig. 6. (A and B) Calculated longitudinal and shear elastic moduli of $(Mg_{0.83},Fe_{0.17})O$ as a function of V_0/V at pressures. The open circles (P–V data) represent the moduli calculated through Eq. 1 using the specimen lengths converted from X-ray diffraction data. The solid circles represent the moduli calculated through Eq. 2 using the specimen lengths observed from the X-radiographic imaging technique. The long dashed lines represent the finite-strain fits using Eqs. 3 and 4.

$$G_0 = M_1 \tag{5}$$

$$K_{S0} = L_1 - \frac{4}{3}G_0 \tag{6}$$

$$G'_0 = \frac{1}{3}\frac{(5M_1 - M_2)}{K_{S0}} \tag{7}$$

$$K'_{S0} = \frac{1}{3}\frac{(5L_1 - L_2)}{K_{S0}} - \frac{4}{3}G'_0 \tag{8}$$

as rearranged from Davies and Dziewonski [32] in terms of the linear compression S, and L_i and M_i are the fitting coefficients. These fitting coefficients are used to calculate the ambient bulk and shear moduli (K_{S0} and G_0) and their pressure derivatives (K_{S0}' and G_0') via Eqs. 5–8 and the results are tabulated in Table 2 for the two different length measurement methods (Eqs. 1 and 2). As suggested by the two sets of data in Fig. 6, these two solutions for K_{S0}, G_0 K_{S0}' and G_0' are the same within the uncertainties.

It has been common practice in our laboratory and others to utilize the finite-strain formulation of Davies and Dziewonski [30] to fit measured ultrasonic data to obtain the elastic parameters. However, in most of these previous studies, it was necessary to determine the pressure via an internal standard (e.g. NaCl) or based on previous calibrations using a fixed point for phase transitions (e.g. in Bi and ZnTe). By combining the ultrasonic determination of travel times and the measurement of specimen volumes and lengths by the techniques of X-ray diffraction and radiographic imaging, this fitting process can be conducted without knowledge of the cell pressure by using V_0/V of the specimen as the independent variable. In this manner, it is possible to eliminate the systematic errors introduced by the pressure scale in the observed elastic parameters (see also earlier experiments in our laboratory on MgO single crystals [18]).

4. Comparison with previous results

In this study, the elastic properties at zero-pressure (K_{S0} and G_0) were obtained from the finite-strain EoS fit (Eqs. 5 and 6). We take these values of K_{S0} and G_0 to be representative of those of the fully-dense, crack-free material, and use these data for comparison with the results of previous studies and in calculations of the properties of mineralogical assemblages for the lower mantle (see below).

In Table 2, we compare our new data with those obtained from previous ultrasonic studies of (Mg,Fe)O single crystals [6] and polycrystalline specimens [4]. Within the mutual uncertainties,

Table 2
Comparison of the elasticity of (Mg,Fe)O and MgO

	K_S	G	K_S'	G'
	GPa			
$(Mg_{0.83},Fe_{0.17})O^{this\ study}$, K533				
X-ray data	165.6(12)	112.5(2)	4.14(20)	1.88(5)
Image data	165.6(12)	112.5(2)	4.20(20)	1.90(6)
$(Mg_{0.85},Fe_{0.15}O$				
[4]	168(4)	109(1)		
[6]	166(3)	109(2)		
MgO				
[31]	162.5	130.0	4.13	2.5

our K_{S0} and G_0 data for $(Mg_{0.83},Fe_{0.17})O$ agree with the values determined in the single-crystal study of Jacobsen et al. [6] and for the polycrystalline specimen of Jackson et al. [9] for the composition with ~15% FeO.

When our data are compared with those for MgO [31] (Table 2), it is clear that K_{S0} is insensitive to the addition of 17 mol% FeO in ferropericlase, but G_0 is reduced by ~14%. The value of K_{S0}' for our specimen of ferropericlase is considered to be identical with that for pure MgO [31]. This insensitivity of K_{S0}' to the FeO content is consistent with an earlier report of Bonczar and Graham [5] for data with less than 30 mol% FeO, observed at low pressure (0.5 GPa).

By contrast with the behavior observed for K_{S0}', the pressure derivative of the shear modulus (G_0') is very sensitive to the substitution of FeO in ferropericlase, decreasing by 24% with the addition of 17 mol% FeO. This behavior recalls the strong dependence of G_0 on the FeO content first observed by Jackson et al. [4], in (Mg,Fe)O polycrystalline specimens, and later confirmed by Jacobsen et al.'s single-crystal data [6]. Furthermore, in their study of wüstite, Jackson et al. [32] measured $G_0' = 1.7$, which suggested that addition of FeO would markedly reduce the pressure derivative of G in ferropericlase.

5. Discussion and summary

Some further insight into the behavior of the elastic properties in the (Mg,Fe)O solid solution series can be obtained by utilizing the recent single-crystal data of Jacobsen et al. [6]. Although this study demonstrated that the individual elastic moduli C_{ij} (C_{11}, C_{12}, C_{44} for the cubic symmetry) exhibited a different compositional dependence (e.g. C_{11} decreases, while C_{12} increases), the bulk modulus, calculated using $K_S = (C_{11}+2C_{12})/3$, is independent of the Fe content for compositions with less than 25 mol% FeO. On the other hand, the two independent shear modes (C_{44} and $C' = (C_{11}-C_{12})/2$) both decrease with increasing Fe content, resulting in a strong reduction in the shear modulus, as observed in Jacobsen et al. (figure 10 in [6]). A similar behavior was observed by Jackson et al. [32] for the pressure derivatives of the elastic moduli (C_{ij}') of wüstite, suggesting that Fe has a pronounced effect on G' but little effect on K_S'. As a result, we suggest that the Fe content in the ferropericlase phase within the mantle composition (from ~10 to 20 mol%) may have little effect on compressional properties (K_S and K_S'), but strong effect on shear mode properties (G and G').

Previous authors have shown that the pyrolite compositional model gives acceptable agreement with seismic profiles for the Earth's lower mantle, using measured or assumed values of the thermoelastic properties of $MgSiO_3$ perovskite and (Mg,Fe)O ferropericlase, with reasonable temperatures as starting point (foot) for the mantle adiabat (1600~1700 K). In this section, we illustrate the impact of our new data for ferropericlase on calculations of this type.

As a result of the observed behavior of K_0 and K_0', the density (ρ) and seismic parameter ($\varphi = K_S/\rho = V_P^2 - 4/3\,V_S^2$) profiles at lower mantle conditions calculated from the current (Mg,Fe)O data would not vary from those calculated using K_0 and K_0' from MgO, as has been done in previous studies (e.g. Jackson [33]). This assumes that the temperature effect on the end-member and Fe-bearing phases for bulk modulus is the same, which is justified based on the experimental evidence from the studies of equation of state of (Mg,Fe)O with higher Fe content (up to 40 mol%) [8,9]. Our calculations of bulk moduli also ignore any variation of the Fe partitioning between the perovskite and ferropericlase phases with depth

[1,3]; recent modelling by Kiefer et al. [34] indicates that the bulk moduli of (Mg,Fe)SiO_3 perovskite depend only weakly on Fe content. In contrast, for modelling the shear properties of lower mantle mineral assemblages, the situation is complicated by the strong dependence of G_0 and G_0' for ferropericlase on Fe content; the first-principle calculation of Kiefer et al. [34] suggests that the Fe content also reduces slightly the shear modulus of (Mg,Fe)SiO_3 perovskite. In this circumstance, the Mg/Fe partitioning between Mg-rich perovskite and ferropericlase phases needs to be taken into account in the calculation of S wave properties of the lower mantle.

Based on previous experiments [2,3], $(Mg_{0.83},Fe_{0.17})O$ would be a probable composition for ferropericlase at the top of the lower mantle. Here, to illustrate the implication of these results, we compare the sound velocities of a pyrolite mantle at 660 km depth using: (a) MgO data [31] for the ferropericlase phase; and (b) the properties measured in this study for $(Mg_{0.83},Fe_{0.17})O$. In both cases, we assume that the temperature derivatives are identical; the lack of experimental data necessitates this approach. We find that the P, S wave velocities calculated for depths just below the 660 km for a pyrolite composition are lowered by 0.8 and 2.3%, respectively, because of the effect of iron in the ferropericlase phase. The consequence of these new calculations based on our data is that the magnitude of the calculated velocity jumps across 660 km is reduced by $\sim$11% for P wave and $\sim$20% for S wave, if this discontinuity is considered as a phase transformation boundary only (ringwoodite $\rightarrow$ perovskite+ferropericlase).

This study has demonstrated the importance of Fe effect on the elastic properties of the lower mantle mineralogical phase assemblages. This is especially critical in modelling the shear elastic properties using the ferropericlase phase, even though this phase occupies only $\sim$20% by volume in a pyrolite lower mantle. Moreover, the shear mode properties may serve as a better 'amplifier' to distinguish the competing compositional models of the lower mantle because they are sensitive to the Fe content (this study, [34]). To more fully test these competing models, further investigations of the temperature dependence of the elasticity of (Mg,Fe)O and the compositional substitutions (i.e. Al and Fe) in the Mg-rich perovskite phase will give better constraints on the composition of the lower mantle.

Acknowledgements

We thank Y. Xu for providing the starting materials and K. Woody for analyzing of the chemical composition of the specimens. We also thank I. Jackson and an anonymous reviewer for their constructive comments that improved the manuscript. This study is supported by the National Science Foundation under the Grants EAR9980451 to R.C.L. and EAR0003340 to B.L. The in situ X-ray experiment was carried out at the X-17B1 beam line of National Synchrotron Light Source (NSLS), which is supported by the US Department of Energy, Division of Materials Sciences and Division of Chemical Sciences, under Contract No. DE-AC02-76CH00016.*[BW]*

References

[1] H.K. Mao, G. Shen, R.J. Hemley, Multivariable dependence of Fe–Mg partitioning in the lower mantle, Science 278 (1997) 2098–2100.
[2] B.J. Wood, Phase transformations and partitioning relations in peridotite under lower mantle conditions, Earth Planet. Sci. Lett. 174 (2000) 341–354.
[3] D. Andrault, Evaluation of (Mg, Fe) partitioning between silicate perovskite and magnesiowüstite up to 120 GPa and 2300K, J. Geophys. Res. 106 (2001) 2079–2087.
[4] I. Jackson, R.C. Liebermann, A.E. Ringwood, The elastic properties of $(Mg_X, Fe_{1-X})O$ solid solutions, Phys. Chem. Miner. 3 (1978) 11–31.
[5] L.J. Bonczar, E.K. Graham, The pressure and temperature dependence of the elastic properties of polycrystal magnesiowüstite, J. Geophys. Res. 87 (1982) 1061–1078.
[6] S.D. Jacobsen, H.-J. Reichmann, H.A. Spetzler, S.J. Mackwell, J.R. Smyth, R.J. Angel, C.A. McCammon, J. Geophys. Res. 107 (2002) 10.1029/2001JB000490. Structure and elasticity of single-crystal (Mg,Fe)O and a new method of generating shear wave for gigahertz ultrasonic interferometry.
[7] P. Richet, H.-K. Mao, P.M. Bell, Bulk moduli of magnesiowüstite from static compression experiments, J. Geophys. Res. 94 (1989) 3037–3045.
[8] Y. Fei, H.-K. Mao, J. Shu, J. Hu, P-V-T equation of state

magnesiowüstite ($Mg_{0.6}Fe_{0.4}$)O, Phys. Chem. Miner. 18 (1992) 416–422.
[9] J. Zhang, P. Kostak Jr., Thermal equation of state of magnesiowüstite ($Mg_{0.6}$ $Fe_{0.4}$)O, Phys. Earth Planet. Int. 129 (2002) 301–311.
[10] B. Li, G. Chen, G.D. Gwanmesia, R.C. Liebermann, Sound velocity measurements at mantle transition zone conditions of pressure and temperature using ultrasonic interferometry in a multi-anvil apparatus, in: M.H. Manghnani, T. Yagi (Eds.), Properties of Earth and Planetary Materials at High Pressure and Temperature, American Geophysical Union, Washington, DC, 1998, pp. 41–61.
[11] R. Truell, C. Elbaum, B.B. Chick, Ultrasonic Methods in Solid State Physics, Academic Press, New York, 1969, 77 pp.
[12] I. Jackson, H. Niesler, D.J. Weidner, Explicit correction of ultrasonically determined elastic wave velocities for transducer-bond phase shifts, J. Geophys. Res. 86 (1981) 3736–3748.
[13] R.K. Cook, Variation of elastic constants and static strains with hydrostatic pressure: A method for calculation from ultrasonic measurements, J. Acoust. Soc. Am. 29 (1957) 445–449.
[14] S.M. Rigden, I. Jackson, H. Niesler, A.E. Ringwood, R.C. Liebermann, Pressure dependence of the elastic wave velocities for Mg_2GeO_4 spinel to 3 GPa, Geophys. Res. Lett. 15 (1988) 605–608.
[15] J. Kung, S.M. Rigden, I. Jackson, Silicate perovskite analogue $ScAlO_3$: temperature dependence of elastic moduli, Phys. Earth Planet. Int. 120 (2000) 299–314.
[16] R.C. Liebermann, G. Chen, B. Li, G.D. Gwanmesia, J. Chen, M.T. Vaughan, D.J. Weidner, Sound velocity measurements in oxides and silicates at simultaneous high pressure and temperatures using ultrasonic techniques, in multi-anvil apparatus in conjunction with synchrotron X-radiation determination of equation of state, Rev. High Pressure Sci. Tech. 7 (1998) 75–78.
[17] R.C. Liebermann, B. Li, Elasticity at high pressures and temperatures, in: R.J. Hemley (Ed.), Ultrahigh Pressure Mineralogy: Physics and Chemistry of the Earth's Deep Interior, Reviews in Mineralogy 37, Mineralogical Society of America, Washington, DC, 1998, pp. 459–492.
[18] G. Chen, R.C. Liebermann, D.J. Weidner, Elasticity of single-crystal MgO to 8 gigapascals and 1600 kelvin, Science 280 (1998) 1913–1916.
[19] B. Li, R.C. Liebermann, D.J. Weidner, Elastic moduli of wadsleyite (β-Mg_2SiO_4) to 7 gigapascals and 873 kelvin, Science 281 (1998) 657–677.
[20] Y.D. Sinelnikov, G. Chen, D.R. Neuville, M.T. Vaughan, R.C. Liebermann, Ultrasonic shear wave velocities of $MgSiO_3$ perovskite at 8 GPa and 800K and lower mantle composition, Science 281 (1998) 677–679.
[21] B. Li, D.J. Weidner, In-situ elastic wave velocity measurements on unquenchable mantle phases using ultrasonics and X-ray radiography/diffraction at high P and T, EoS Transactions, AGU, Spring Meeting, Vol. 18, No. 19, 2000, p. S35.
[22] B. Li, I. Jackson, T. Gasparik, R.C. Libermann, Elastic wave velocity measurement in multi-anvil apparatus to 10 GPa using ultrasonic ultrasonic interferometry, Phys. Earth Planet. Int. 98 (1996) 79–91.
[23] G.D. Gwanmesia, R.C. Liebermann, F. Guyot, Hot-pressing and characterization of polycrystals for β-Mg_2SiO_4 for acoustic velocity measurements, Geophys. Res. Lett. 17 (1990) 1331–1334.
[24] G.D. Gwanmesia, R.C. Liebermann, Polycrystals of high-pressure phases of mantle minerals: Hot-pressing and characterization of physical properties, in: Y. Syono, M.H. Manghnani (Eds.), High Pressure Research: Applications to Earth and Planetary Sciences, Terra Scientific Publishing Co., Tokyo/American Geophysical Union, Washington, DC, 1992, pp. 117–135.
[25] G.D. Gwanmesia, B. Li, R.C. Liebermann, Hot pressing of polycrystals of high-pressure phases of mantle minerals in multi-anvil apparatus, Pure Appl. Geophys. 141 (1993) 467–484.
[26] H. Niesler, I. Jackson, Pressure derivatives of elastic wave velocities from ultrasonic interferometic measurements on jacketed polycrystals, J. Acoust. Soc. Am. 86 (1989) 1573–1585.
[27] J. Kung, R. Angel, N. Ross, Elasticity of $CaSnO_3$ at high pressure, Phys. Chem. Miner. 28 (2001) 35–43.
[28] D.J. Weidner, M.T. Vaughan, J. Ko, Y. Wang, X. Liu, A. Yeganeh-Haeri, R.E. Pacalo, Y. Zhao, Characterization of stress, pressure and temperature in SAM85, A DIA type high pressure apparatus, in: Y. Syono, M.H. Manghnani (Eds.), High-Pressure Research: Application to Earth and Planetary Sciences, Geophysical Monograph 67, Terra Scientific Publishing Co., Tokyo/American Geophysical Union, Washington, DC, 1992, pp. 13–17.
[29] M. Vaughan, J. Chen, L. Li, D. Weidner, B. Li, Use of X-ray image techniques at high pressure and temperature for strain measurements, in: M.H. Manghnani, W.J. Nellis, M.F. Nicol (Eds.), Science and Technology of High Pressure, Universities Press, Hyderabad, 2000, pp. 1097–1098.
[30] G.F. Davies, A.M. Dziewonski, Homogeneity and constitution of the Earth's lower mantle and outer core, Phys. Earth Planet. Int. 10 (1975) 336–343.
[31] I. Jackson, H. Neisler, The elasticity of periclase to 3 GPa and some geophysical implications, in: S. Akimoto, Manghnani, M.H. (Eds.), Advances in Earth and Planetary Sciences 12, High-pressure Research in Geophysics, Centre for Academic Publications, 1982, pp. 93–113.
[32] I. Jackson, S.K. Khanna, A. Revcolevschi, J. Berthon, Elasticity, shear mode softening and high-pressure polymorphism of wüstite $Fe_{1-X}O$, J. Geophys. Res. 95 (1990) 21671–21685.
[33] I. Jackson, Elasticity, composition and temperature of the Earth's lower mantle: a reappraisal, Geophys. J. Int. 134 (1998) 291–311.
[34] B. Kiefer, L. Stixrude, R.M. Wentzcovitch, Elasticity of $(Mg_{1-X},Fe_X)SiO_3$-perovskite at high pressures, Geophys. Res. Lett. 29 (2002) 10.1029/2002GLO14683.